Antipodal Hotspots and Bipolar Catastrophes: Were Oceanic Large-Body Impacts to Blame?

Jonathan T. Hagstrum *U.S. Geological Survey, 345 Middlefield Road, MS 937, Menlo Park, CA 94025; jhag@usgs.gov*

#V51B-0581

1. Introduction

The 'standard' plume model has been rejected by some authors (see www.mantleplumes.org) in favor of an alternate model in which hotspots were caused by plate-related stresses that fractured the lithosphere allowing melt to reach the surface from shallow heterogeneous sources. Although many hotspots are presently associated with lithospheric fractures, there are still some aspects of hotspot origins (e.g., radial dike swarms, continental rifting, see **Fig. 1**) that appear more compatible with large plume-like events.

2. Methods

One important aspect of the hotspot distribution that has received little attention is its antipodal character. This study was undertaken to examine and test the antipodal character of Earth's hotspot distribution, to evaluate a possible mechanism of antipodal hotspot formation, and to briefly explore the geologic implications of such a mechanism of hotspot origins.

A list of the 45 most prominent or 'primary' hotspots, common to most published lists, was constructed (circles, **Fig. 2**; bold type, **Tables 1 & 2**). These hotspots were assumed to have formed from the largest causal events. Within this group, however, the greatest causal events were most likely those associated with initial flood basalt eruptions (**Table 1**). Antipodal sites for the list of primary hotspots were determined from their present surface locations assuming that each hotspot directly overlies its melting anomaly in the upper mantle. Of critical importance to defining antipodal hotspot pairs is the drift of individual hotspots over time. Plate reconstruc-tions have shown average drift rates of 10 to 20 mm/yr between hotspots in the Pacific and Atlantic and Indian Oceans [*Molnar & Stock*, Nature 1987].

Figure 1. CAMP dike swarm

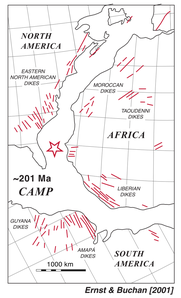

Ernst & Buchan [2001]

3. Antipodal 'primary' and 'secondary' hotspots

Comparisons of initiation ages for antipodal hotspot pairs were made to determine whether or not they formed contemporaneously (**Tables 1 & 2**). Exact ages for hotspots, however, are often difficult to ascertain or are unknown, particularly for those oceanic hotspots where part of their track has been subducted. Usually, at least minimum ages are available for each hotspot of an antipodal pair so that general comparisons could be made.

Seven of the eight primary hotspots, most clearly associated with young large igneous provinces (LIPs), have near-antipodal, mostly primary, hotspots that could initially have been exactly antipodal within relatively conservative drift limits (**Table 1**). Drift limits were calculated assuming contemporaneous antipodal origins at the time of the initial flood basalt eruptions. Comparisons of the ages for many of the antipodal hotspot pairs in **Tables 1 & 2** show that they are similar within <10 Myr, or, for those with only minimum ages, that their possible age ranges overlap (**Fig. 3**).

Comparisons between primary and secondary hotspots are continued in **Table 2** and elsewhere (secondary hotspots are gray symbols in **Fig. 2**). Only 4 of the 45 primary hotspots are without near-antipodal volcanic features, and antipodes for these 4 hotspots would have been located in the ancestral Pacific Ocean. Moreover, there are few contradictions between well-defined ages within all the pairs (<10 Myr), and no flood-basalt related hotspots are antipodal to one another.

The antipodal hotspot comparisons are illustrated in **Figure 4** (see also **Fig. 2**), where antipodal locations of all hotspots are plotted (**Tables 1 & 2**). Note that relatively few hotspots project onto continental crust at their antipodes, particularly those presently situated on continental crust (black symbols). The main concentration of continental hotspots in Africa, above the African 'superswell', projects onto the concentration of hotspots above the Pacific 'superswell' (**Fig. 5**).

Figure 4. Antipodes of hotspot locations

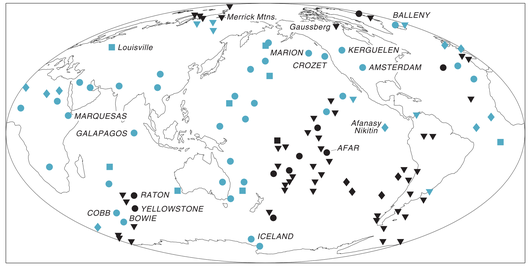

Table 1. Flood basalt provinces, related hotspots, and antipodal hotspots

Flood Basalt Province	Age (Ma)	Related hotspot	Location Lat.(°)	Location Lon.(°)	Antipodal hotspot	Age (Ma)	Location Lat.(°)	Location Lon.(°)	Ang. Dist.(°)	Drift (mm/yr)
Columbia River	~17-15	**Yellowstone**	44 N	249 E	**Kerguelen**	~29-24	49 S	69 E	175	~19
Ethiopian	~31-29	**Afar**	11 N	43 E	**Marquesas**	~36	10 S	222 E	179	~3
North Atlantic	~62-58	**Iceland**	65 N	343 E	**Balleny**	>36	67 S	163 E	178	~4
Deccan	~67-64	**Réunion**	21 S	56 E	**Guadalupe**	>25	19 N	249 E	174	~10
Madagascar	~90-84	**Marion**	47 S	38 E	**Bowie**	>30	53 N	225 E	173	~9
Caribbean-Colombian	~90-87	**Galápagos**	0 N	269 E	Nikitin	~80-73	3 S	83 E	173	~9
Kerguelen-Rajmahal	~115-86	**Amsterdam(?)**	38 S	78 E	**Raton**	?	36 N	256 E	177	~3
Paraná-Entendeka	~134-129	**Tristan**	37 S	348 E	*Pacific?*	*na*	*na*	*na*	*na*	*na*

Figure 2. Hotspot locations

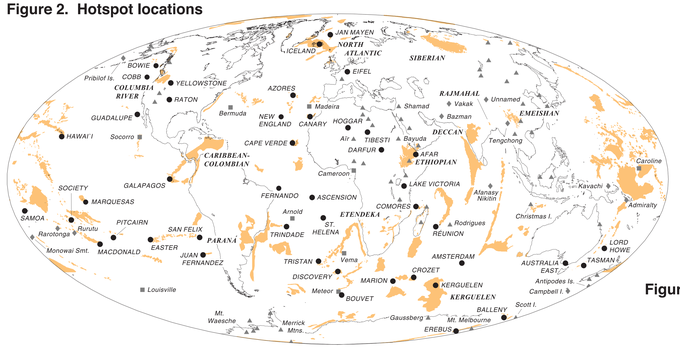

Table 2. Other near-antipodal hotspots on the Earth

Oceanic site	Location Lat.(°)	Location Lon.(°)	Age (Ma)	Antipodal site	Location Lat.(°)	Location Lon.(°)	Age (Ma)	Ang. Dist.(°)	Drift (mm/yr)	Dist. to next hs(°)
Jan Mayen	71 N	352 E	<50[5]	**Mt. Erebus**	77 S	167 E	~40[6]	174	~17	7 / 3
Lord Howe	31 S	159 E	>50[8]	**Canary**	28 N	344 E	~65[8]	175	~9	8 / 5
Cobb	47 N	229 E	>40[8]	**Crozet**	45 S	51 E	>20[7]	178	<6	7 / 9
Tasman	39 S	156 E	>50[8]	**Azores**	38 N	332 E	>60?[5]	177	<6	8 / 10
New England	28 N	327 E	>60?[7]	**E. Australia**	38 S	143 E	>50[8]	169	<20	11 / 10
Hawai`i	19 N	205 E	>100[8]	**Lake Victoria(?)**	3 S	36 E	?	161	<26	5 / 33
Pribilof Is.	57 N	190 E	~2[10]	**Bouvet**	54 S	3 E	>1[11]	175	—	6 / 2
Society	18 S	211 E	~5[8]	Bayuda	18 N	34 E	~4?[12]	177	~66	6 / 8
Pitcairn	26 S	230 E	~8[8]	Bazman-Taftan	28 N	61 E	>2[13]	170	—	9 / 8
Ewing Crater*	14 N	222 E	>7-11[14]	**Comores**	12 S	43 E	>8[15]	175	~69	17 / 6
Samoa	14 S	187 E	~14[8]	Air Massif	18 N	9 E	~9?[16]	176	~32	13 / 6
Macdonald	29 S	220 E	~19[17]	Harr. as Shamad	33 N	37 E	~16?[18]	175	~29	9 / 6
Rarotonga	22 S	201 E	~1[17]	**Tibesti**	21 N	17 E	~17[19]	176	~60	8 / 4
Kavachi	9 S	158 E	?	**Cape Verde**	16 N	335 E	~20[8]	172	~44	12 / 14
Juan Fernandez	34 S	278 E	>30[8]	Unnamed *(China)*	36 N	92 E	?	175	<19	8 / 12
San Felix	26 S	280 E	>30[8]	Tengchong	25 N	98 E	>18[20]	178	<7	8 / 5
Admiralty Is.	3 S	147 E	?	**Fernando**	4 S	328 E	>30[7]	173	<26	12 / 15
Rurutu	24 S	209 E	>10[21]	**Darfur**	13 N	24 E	~35[16]	168	~38	6 / 10
Monowai Smt.	26 S	183 E	?	**Hoggar**	23 N	6 E	~35[16]	176	~13	13 / 6
Socorro	19 N	249 E	>25[8]	Rodrigues	20 S	63 E	~36[22]	174	<19	12 / 7
Campbell I.	52 S	169 E	>11[23]	**Eifel**	50 N	7 E	~40[8]	169	~31	2 / 5
Nikitin	3 S	83 E	~80-73[24]	**Galápagos**	0 N	269 E	~90[2]	173	~9	24 / 27
Caroline	5 N	164 E	>30[17]	**St. Helena**	8 S	346 E	~100[8]	166	~16	15 / 11
Easter	27 S	251 E	>100[8]	Vakak Group	34 N	68 E	?	173	<8	8 / 19

*see Table 4

Age references:
[1] Nicolaysen et al., EPSL 174 (2000) 313-328.
[2] Ernst & Buchan (Eds.) GSA Spec. Pap. 352 (2001) 483-575.
[3] Crough & Jarrard, JGR 86 (1981) 11,763-11,771.
[4] Schlanger et al., JGR 89 (1984) 11,261-11,272.
[5] Morton & Parson (Eds.) GS Spec. Pub. 39 (1988) 85-93.
[6] LeMasurier & Thomson (Eds.) AGU, Ant. Res. Ser. 48 (1990) 81-88.
[7] Duncan & Richards, Rev. Geophys. 29 (1991) 31-50.
[8] Steinberger, JGR 105 (2000) 11,127-11,152.
[9] Luyendyk & Rennick, GSA Bull. 88 (1977) 1347-1356.
[10] Cox et al., GSA Bull. 77 (1966) 883-910.
[11] LeMasurier & Thomson (Eds.) AGU, AR Ser. 48 (1990) 405-410.
[12] Almondet al., J. Afr. Earth Sci., 2 (1984) 233-245.
[13] Gansser, Edogae geol. Helv. 64 (1971) 319-334.
[14] Abbott et al., Eos Trans., AGU 84 (2003) P52A-0472.
[15] Nougier et al., J. Afr. Earth Sci. 5 (1986) 135-145.
[16] Macgregor et al. (Eds.) GS Spec. Pup. 132 (1998) 231-263.
[17] Clouard & Bonneville, Geology 29 (2001) 695-698.
[18] Segev, Tectonophys. 325 (2000) 257-277.
[19] Vincent, written communication, 2003.
[20] Zhiguo et al., Geothermics 16 (1987) 283-297.
[21] Chauvel et al., Chem. Geol. 139 (1997) 125-143.
[22] Baxter et al., Contrib. Mineral. Petrol. 89 (1985) 90-101.
[23] LeMasurier & Thomson (Eds.) AGU, Ant. Res. Ser. 48 (1990) 474-475.
[24] Krishna, EPSL 209 (2003) 379-394.
[25] http://www.unb.ca/passc/ImpactDatabase/
[26] Richards et al. (Eds.), AGU, Geophys. Mono. 121 (2000) 339-357.
[27] Notholt et al.(Eds.), Phosphate Deposits... 2 (1989) 558-563.
[28] Luyendyk & Rennick, GSA Bull. 88 (1977) 1347-1356.
[29] Nicolaysen et al., EPSL 174 (2000) 313-328.
[30] Lonsdale, JGR 93 (1988) 3078-3104.

Figure 3. Hotspot age ranges (± 10 Myr)

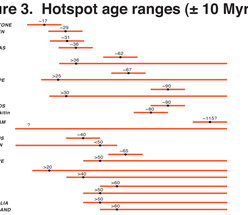

Table 3. Primary hotspots vs. random distributions

Limit (°) (L_{MAX})	Primary pairs (N_P)	$p(L_{MAX})$	$p(L_{MAX})$ ages	$p(L_{MAX})$ >20° lat.	$p(L_{MAX})$ >20° lat.; ages
2.0	2	0.031	0.0141	0.068	0.033
3.0	4	0.002	0.0005	0.013	0.004
4.0	5	0.004	0.0006	0.008	0.002
5.0	6	0.003	0.0004	0.021	0.001
6.0	7	0.004	<0.0001	0.023	0.002
7.0	7	0.018	0.0011	0.082	0.008
8.0	9	0.006	<0.0001	0.038	0.002
9.0	10	0.004	0.0002	0.061	0.006
10.0	11	0.003	0.0003	0.030	0.005

4. Monte Carlo simulations

The number of primary hotspot pairs (N_P) within limit values of exact antipodality (L_{MAX}) of 2.0° to 10.0° ranges from 2 to 11 and are listed in **Table 3**. Either 1000 or 10000 random distributions of 45 hotspots were generated to test each null hypothesis, and for each L_{MAX} the fraction (p) of artificial distributions with at least as many antipodal pairs as the primary hotspot list (N_P) was determined. Assuming that the primary hotspots are randomly distributed over the entire Earth's surface, only 3 randomly generated distributions out of 1000 have 11 (N_P) or more antipodal hotspot pairs ($p(L_{MAX})$=0.003) with L_{MAX} set to 10.0°. The randomly distributed null hypothesis, therefore, can be rejected at the >99% confidence level.

The actual age estimates for the primary hotspots (**Fig. 3**) were also randomly associated with the artificially generated hotspots. The assigned ±10 Myr error ranges were more than enough to allow the age estimates of all antipodal pairs in **Table 1** to overlap. For most L_{MAX} values the age-modified null hypothesis can be rejected at >99.9% (p<0.001) confidence level (**Table 3**). Finally, similar null hypotheses were tested in which the artificial hotspot locations were limited to spherical caps (>20° latitude) totaling two-thirds of the Earth's surface area or the area of the oceanic basins. In this case, the null hypothesis without ages can be rejected for most L_{MAX} values at >95% (p<0.05) confidence level, and, that with the ages included, mostly at >99% confidence level (p<0.01; **Table 3**).

Figure 5.

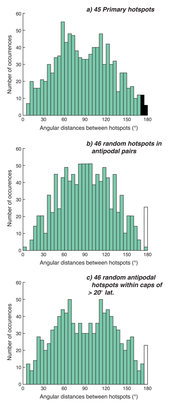

Figure 6. Antipodal focusing of seismic energy

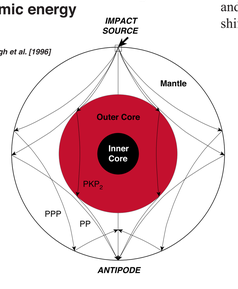

5. Mechanism of antipodal hotspot formation

An inherently antipodal model of hotspot and LIP formation (**Fig. 6**) is proposed in which minor hotspot volcanism is generated at a large-body impact sites and flood-basalt volcanism is triggered antipodally by focused seismic energy [*Boslough et al*., GSA Spec. Pap. 307 1996]. Shock-hydrodynamic simulations used to generate source functions for seismological modeling of the Earth (10-km-diameter asteroid impacting at 20 km/s), show the largest displacements (±10 m at antipode), stresses, and strains in the antipodal lithosphere and upper asthenosphere. Accepting that the upper mantle is likely hotter and more fertile than generally presumed in 'standard' mantle plume models (www.mantleplumes.org), lithospheric fracturing by focused seismic energy from large-body impacts might have played a major role in the formation of antipodal flood basalts. Shock wave attenuation is expected to be higher in the tectosilicates found primarily in continental and not oceanic crust. Large oceanic impacts are thus inferred to have been mostly responsible for the formation of antipodal hotspot pairs (**Fig. 7; Table 4**). Oceanic large-body impacts (10-km-diameter asteroid) also differ from continental impacts in that the bulk of their ejecta is high-velocity water vapor containing only small amounts of crustal material [*Roddy et al*., Int. J. Impact Eng. 1987], and that they generate megatsunami capable of widespread catastrophic effects [*Ahrens & O'Keefe*, JGR 1983].

6. Implications of antipodal hotspot model

Global mass extinctions have also been associated with continental LIP events, as well as to large-body impacts, rapid regressive and transgressive changes in sea level, and abrupt changes in ocean chemistry. Megatsunami in the 'oceanic' hemisphere and vast quantities of noxious gases (CO_2, SO_2, HCl) from flood basalt eruptions in the 'continental' hemisphere might have been responsible for the profound environmental changes at ~68-67 Ma triggering the Cretaceous/Tertiary (K/T) transition. A large drop then rise in eustatic sea level (**Fig. 8**), a distinct positive spike in the $^{87}Sr/^{86}Sr$ ratio of sea water, and extinctions of the rudistid clam reefs, inoceramid bivalves, belemnites, and shallow-water ammonite species all occurred. Climate change is also indicated by fossil plant communities in the *Aquilapollenites* Province of western North America and Eastern Siberia.

The Permian/Triassic (P/T) transition comprised two distinct events separated in time by ~5 Myr (**Fig. 9**). The first extinction pulse occurred along with eruption of the Emeishan LIP of southern China (**Fig. 2**) as sea level apparently regressive underwent and transgressive changes. During the subsequent end-Permian event, the Siberian Traps were erupted and sea level apparently dropped, then returned, by perhaps the largest amount in Phanerozoic time. Thus, two large oceanic impacts close together in space and time might have triggered the end-Permian LIPs, and caused the apparent changes in sea level and shifts in ocean chemistry.

Figure 7. Known impact structures

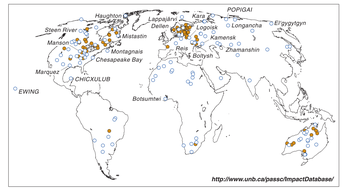

Figure 8. K/T boundary at Braggs, Alabama

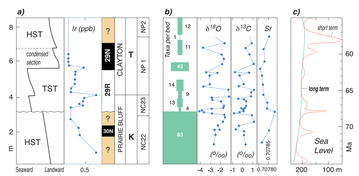

Figure 9. Apparent P/T sea level changes

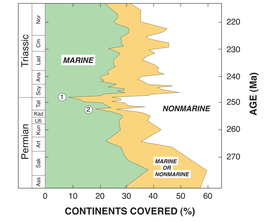

Table 4. Largest well-dated impact craters (>10 km; <100 Ma[25]) and nearest antipodal hotspot

Impact structure	Location Lat.(°)	Location Lon.(°)	Age (Ma)	Diam. (km)	African coord.[26] Lat.(°)	African coord.[26] Lon.(°)	Antipodal hotspot	Location Lat.(°)	Location Lon.(°)	Age (Ma)	Afr. coord.[26] Lat.(°)	Afr. coord.[26] Lon.(°)	Dist. (°)	Drift (mm/yr)
Chicxulub *(Mexico)*	21 N	270 E	~65	170	18 N	290 E	Christmas I.	11 S	106 E	>40[27]	5 S	112 E	167	~22
Ewing *(Pacific Ocean)*	14 N	222E	>7-11[14]	~150	11 N	229 E	**Comores**	12 S	43 E	>8[15]	11 S	44 E	175	~69
Popigai *(Russia)*	72 N	111 E	~36	100	76 N	127 E	Merrick Mtns.	75 S	288 E	?[6]	78 S	298 E	177	~9
Montagnais *(Canada)*	43 N	296 E	~51	45	41 N	311 E	**E. Australia**	38 S	143 E	>50[8]	39 S	142 E	171	~20
Kamensk *(Russia)*	48 N	41 E	~49	25	53 N	40 E	Louisville	51 S	219 E	>70[30]	54 S	219 E	179	~2
Haughton *(Canada)*	75 N	270 E	~23	24	73 N	277 E	Gaussberg	68 S	89 E	~20[6]	65 S	87 E	171	~43
Boltysh *(Ukraine)*	49 N	32 E	~65	24	56 N	29 E	Louisville	51 S	219 E	>70[30]	54 S	232 E	167	~22

Age references (see Table 2); see also Figure 7.